Global and low-cost topographic data to support flood studies

Yan, Kun; Neal, Jeffrey C.; Solomatine, Dimitri P.; Di Baldassarre, Giuliano

Citation (APA)
Yan, K., Neal, J. C., Solomatine, D. P., & Di Baldassarre, G. (2023). Global and low-cost topographic data to support flood studies. In J. F. Shroder, G. Di Baldassarre, & P. Paron (Eds.), *Hydro-Meteorological Hazards, Risks, and Disasters* (2 ed., pp. 85-102). (Hazards and Disasters Series; Vol. 5). Elsevier. https://doi.org/10.1016/B978-0-12-819101-9.00010-8

Important note
To cite this publication, please use the final published version (if applicable).
Please check the document version above.

Chapter 3

Global and low-cost topographic data to support flood studies

Kun Yan[1,5], Jeffrey C. Neal[2], Dimitri P. Solomatine[1,3] and Giuliano Di Baldassarre[1,4]

[1]*IHE-Delft, Institute of Water Education, Delft, The Netherlands;* [2]*School of Geographical Sciences, University of Bristol, Bristol, United Kingdom;* [3]*Water Resources Section, Delft University of Technology, Delft, the Netherlands;* [4]*Department of Earth Sciences, Uppsala University, Uppsala, Sweden;* [5]*Deltares, Delft, the Netherlands*

3.1 Introduction

3.1.1 Growing availability of global earth observation data

The recent catastrophic flood events (e.g., Central Europe, June 2013) encouraged more efforts in flood risk-prevention measures to reduce human losses and economic damages. To this end, modeling and mapping flood inundation processes using hydraulic modeling techniques has become an essential component (de Moel et al., 2009; Van Alphen et al., 2009). The growing availability of distributed remote sensing data has provided a great potential in building and testing flood inundation models in recent years (Bates, 2012; Di Baldassarre and Uhlenbrook, 2012). In addition to the high-resolution digital elevation models (DEMs), which are highly precise but costly, global low-cost products also provide topographic data, such as the DEM derived by the shuttle radar topography mission (SRTM). These topographic data may potentially offer new opportunities to implement flood inundation modeling in data scarce/poor areas. However, SRTM suffers from random noises and radar speckles due to the fact that it utilizes radar-based interferometry technology, which involves the reception of a back-scattered radar signal by two antennae. Speckle adds waviness with amplitudes of ∼1.0 m to SRTM (Falorni et al., 2005). Additionally, vertical accuracy is degraded by its space-borne altitude and its inability to penetrate water surface and dense vegetation (Falorni et al., 2005). Hence, the low accuracy of SRTM (Rabus et al., 2003; Rodríguez et al., 2006) together with all its drawbacks listed above seem that utilizing SRTM data in flood modeling is rather

challenging. However, SRTM is characterized by errors in flat areas lower than the errors occurring in high slope areas (Rodríguez et al., 2006). This feature of the SRTM is beneficial for the potential use of this topographic data to support large-scale inundation modeling as floodplains are usually flat and with a mild slope. In addition, floodplain flow above small-scale topography features, which are usually misrepresented by the SRTM, do not play a dominate role in large-scale flood inundation processes (Bates, 2012).

3.1.2 Recent progress on evaluation of global topographic data in supporting flood modeling

The recent scientific efforts on exploring the potential usefulness of SRTM data in supporting floodplain monitoring at large scale are encouraging. For example, LeFavour and Alsdorf (2005) derived the water-surface slope of Amazon based on SRTM topography and found that accurate main stem discharge values can be estimated with this water-surface slope in this biggest river of the world. Schumann et al. (2010) compared the water surface gradient generated by intersecting SAR image and SRTM DEM to that derived from intersecting SAR image with a high resolution and quality Light Detection And Ranging (LiDAR) DEM on River Po. They found that there the two estimates are remarkably close to each other. Sanders (2007) evaluated diverse public DEMs (including interferometric synthetic aperture radar [IfSAR] and SRTM) for flood inundation modeling and found that airborne IfSAR was not appropriate for flood simulation, while SRTM topography led to a 25% larger flood zone when compared with the high-resolution topography in a steady-flow Santa Clara River application. Schumann et al. (2012) calibrated the hydrodynamic model by using highly accurate water levels on the main channel from the ICESat (Ice, Cloud, and land Elevation Satellite) laser altimeter and validated using multiple satellite acquisitions of the flood area in the forecasting for the Lower Zambezi River in southeast Africa. Results showed that satisfactory parameter values and performance, as well as acceptable prediction skills can be achieved at a very large scale and using coarse grid resolutions. In a recent study (Yan et al., 2013), the design flood profiles derived from hydraulic models based on high resolution and accuracy topography and bathymetry (LiDAR) and hydraulic models based on SRTM data were compared considering all the other major sources of uncertainty that unavoidably affect any modeling exercise. It was found out that the differences between the high resolution topography-based model and the SRTM-based model were not negligible, but within the accuracy that is typically associated with large-scale flood studies. However, the flood event considered in Yan et al. (2013) was confined by the lateral embankments of the River Po, and therefore a one-dimensional (1D) hydraulic model was used in that study. Moreover, studies at different scales mentioned above yield quite different conclusions. Hence, the value of SRTM topography in supporting two-

dimensional (2D) flood inundation modeling remains largely unexplored, particularly for medium−small-sized (with width smaller than 100 m) rivers.

3.1.3 Uncertainties in inundation modeling and probabilistic flood mapping

Many studies have described that there are several sources of uncertainties intrinsic to flood inundation modeling, such as model structure, topographic data, model parameter, and inflow etc (e.g., Aronica et al., 2002; Pappenberger et al., 2006; Di Baldassarre and Montanari, 2009). Among those, topography uncertainty is considered to be one of the major sources of uncertainty. The flood inundation maps are characteristically produced by hydraulic models using deterministic or probabilistic approaches. The deterministic flood maps which are produced by using a fully 2D physically based best-fit model are precise, but potentially wrong, due to the fact that they ignore the above-mentioned uncertainties in inundation modeling. The probabilistic flood maps that explicitly consider various sources of uncertainties are believed to be theoretically more appropriate for visualizing flood hazard (Di Baldassarre et al., 2010), even though their application in flood risk studies is still limited.

3.1.4 Different types of data in constraining uncertainty in flood modeling

Recent advances in airborne and satellite remote sensing allow the parameterization, calibration, and validation of flood inundation models in a distributed manner (Bates, 2004). Hydraulic models are usually tested on flood extent data (e.g., Matgen et al., 2007; Pappenberger et al., 2007; Neal et al., 2013) rather than water level or flow data at particular points as the models may not perform well at the locations away from the gauged points (Bates et al., 2004). As pointed out by Pappenberger et al. (2007), data used to constrain model parameter uncertainty should be consistent with the modeling purpose. For example, models are better to be conditioned on flood extent data if the goal is predicting flood-prone areas, whereas high water marks are preferable if the purpose is estimating design flood profiles (Brandimarte and Di Baldassarre, 2012).

Yet, the use of flood extent data can sometimes be difficult to distinguish between different model parameterization when the flood extent is not sensitive to changes in water level. In addition, flood extents from satellite flood images are usually difficult to obtain. As a matter of fact, the overpass frequency of the satellites which provides high-resolution flood imagery is usually low (e.g., 35 days of repeat cycle for ERS2-SAR, Schumann et al., 2010) even though there are few products with low revisit time recently available (e.g., COSMO-SkyMed offers 12 and 24 h revisit time, García-Pintado et al., 2013). This implies that finding a satellite image at the time of flooding may be

difficult as flood duration time in small—medium catchment is usually shorter than the revisit time of satellite data (Hunter et al., 2007; Schumann et al., 2010). Hydrometric data such as water stages are relatively easier to find. They have a high temporal frequency but are unavoidably sparse in space (Di Baldassarre et al., 2011).

A few scientists have explored the use of different types of data sets to constrain uncertainty in inundation models. For example, Horritt and Bates (2002) tested three hydraulic codes on a 60-km reach of the River Severn, UK, using independent hydrometric and satellite data for model calibration. They found all models are capable of reproducing inundation extent and flood wave travel time to the similar level of accuracy at optimal simulation. However, the predictions of inundation extent are in some cases poor when hydrometric data are used for model calibration. Hunter et al. (2005) calibrated an inundation model against flood images, downstream stage, and discharge hydrographs on a 35-km reach of the River Meuse, the Netherlands. They found that the evaluation of internal predictions of stage also offers considerable potential for reducing uncertainty over effective parameter specification.

3.1.5 The dilemma of downstream water level in hydraulic modeling

In hydraulic modeling, the normal depth (calculated from the water surface slope) is often used as downstream boundary condition. The water surface slope is normally unknown and is often estimated as the average bed slope under the assumption of a Manning's type relationship between water stage and discharge at the downstream end of the river reach. The results of flood inundation models (e.g., water levels, inundation extent) are affected by this assumption, especially when backwater effects are significant. Samuels (1989) proved the practical use of Eq. (3.1) to calculate the backwater length, L, for engineering applications:

$$L = \frac{0.7D}{s_0} \tag{3.1}$$

where D is the bankfull depth of the channel and S_0 is the bed slope. Only a few studies (e.g., Wang et al., 2005; Schumann et al., 2008) have investigated the impact of assuming a certain water surface slope as downstream boundary conditions on the results of 2D hydraulic models, such as inundation extent and water stage. Those impacts can be substantially reduced by extending the model domain and placing the downstream water level sufficiently far away from the points of interest. However, this is not always possible.

In this context, the aim of this chapter is twofold: (1) explore the potentials and limitations of SRTM data in supporting the 2D hydraulic modeling of floods; (2) examine the sensitivity of 2D hydraulic models on the water surface

slope used as downstream boundary as well as the associated value of downstream water levels in constraining uncertainty of flood extent prediction.

3.2 Test site and data availability

The study is carried out on a river system including: (1) the 10-km reach of the River Dee, between Farndon and Iron Bridge, two gauging stations of the Environment Agency of England and Wales (hereafter called the EA); and (2) the 8-km reach of the River Alyn, between the EA gauging station of Pont-y-Capel and the confluence to the River Dee (Fig. 3.1). A high resolution (2 m) LiDAR DEM of this test site is derived by the EA. Surface artifacts such as vegetation and buildings are removed from the raw LiDAR data. The EA also conducts a channel bathymetry ground survey of 36 cross-sections that are incorporated with the LiDAR data on floodplain. Hereafter, this hybrid high-resolution DEM is called LiDAR DEM.

Another DEM of the test site is derived from the SRTM data postprocessed by the Consortium for Spatial Information of the Consultative Group for International Agricultural Research, for example, fills in the no-data holes in the raw SRTM data (Jarvis et al., 2008). The SRTM DEM of the study area is reprojected into 75 m resolution with no speckles and surface artifacts removed. The two DEMs are strongly different, not only in terms of resolution (2 vs. 75 m) but also in terms of accuracy: the vertical accuracy of LiDAR data was of around 10 cm, whereas that of SRTM in Europe was found around 6 m (Rodríguez et al., 2006).

In December 2006, the River Dee underwent a low magnitude flood event (with the return period about two years). In this period, a high-resolution satellite image (ERS-2 SAR, see in Fig. 3.1) was acquired. The ERS-2 SAR image is characterized by a pixel size of 12.5 m and a ground resolution of approximately 25 m. The satellite image was processed by using visual interpretation procedure to derive a flood extent map (Schumann et al., 2009; Di Baldassarre et al., 2010). We reproject this flood extent map into the 20 and 75 m resolution for evaluating the LiDAR-based and SRTM-based models (see below).

3.3 Inundation modeling

The LISFLOOD-FP (Bates and De Roo, 2000) raster-based hydraulic model is used to simulate the flood event in 2006. The main channel widths of River Dee and Alyn are on average 30 and 12 m, respectively, which are much smaller than SRTM DEM cell resolution (i.e., 75 m). Therefore, the subgrid approach of LISFLOOD-FP (Neal et al., 2012), which can represent 1D channels with widths below the grid resolution, is applied for the SRTM-based model. The subgrid approach allows the modeler to specify channel width, channel depth as well as the bank elevation inside each cell, so that it can
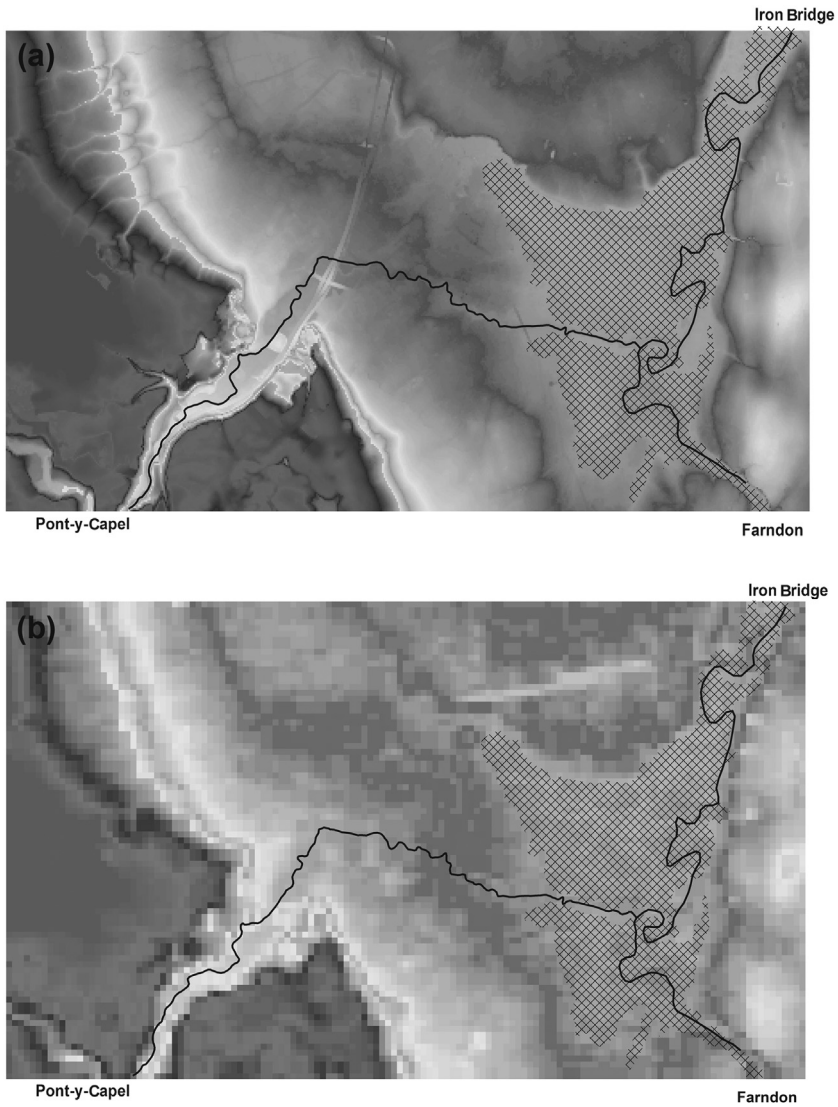
FIGURE 3.1 River Dee between Farndon and Iron Bridge and River Alyn from Pont-y-Capel (black lines); flood extent of 2006 event from ERS2-SAR flood image (crosshatch); (A) LiDAR digital elevation model (DEM) (gray scale); (B) shuttle radar topography mission DEM (gray scale).

better emulate flood propagation in the main channel for coarse resolution models. It was proved to change the floodplain inundation dynamics significantly and increase simulation accuracy in terms of water levels, wave propagation speed, and inundation extent compared with the pure 1D channel model or 2D floodplain model of LISFLOOD-FP (Neal et al., 2012). The

subgrid approach uses the floodplain flow model of Bates et al. (2010), which introduced the local inertial term to the diffusive wave equation to significantly reduce the computation cost. However, computational cost can still be high for fine resolution (e.g., 1−10 m) grids. Therefore, the 2 m LiDAR DEM is aggregated into 20 m resolution to reduce the model computational time. The key topographic features such as embankments are manually identified in the aggregated DEM.

The channel-bed elevation of SRTM topography is found to be overall overestimated in the study area. This is due to the fact that radar wave cannot penetrate water surface to detect the channel-bed elevation and the channel is typically smaller than an SRTM pixel. Therefore, we improve the SRTM channel-bed elevation by using the boat survey data. However, the combination of boat-surveyed, channel-bed elevation and overestimated SRTM floodplain topography results in a very deep channel depth (around 8−10 m). As one of the main purposes of inundation modeling is to predict the flood extent correctly, we use the surveyed channel depth (bank elevation subtract bed elevation) to replace the SRTM channel depth rather than directly replacing SRTM bed elevation by the surveyed bed elevation.

Two hydraulic models (LiDAR and SRTM-based) are built to simulate the 2006-year flood event. The observed discharge hydrograph starting on December 6, 2006 at 11:00 h (around 144 h before the satellite overpass) is used as upstream boundary condition. A normal depth with the water surface slope (estimated as the average bed slope) is applied as the downstream boundary condition.

In this study, two types of observations are available for the model evaluation: (1) spatially distributed binary flood extent and (2) at-a-point time series of flood water stages (Iron Bridge). The simulated inundation areas are compared to the observed flood extent map (derived from the ERS2-SAR satellite imagery, Fig. 3.1) using the performance measure, F (Aronica et al., 2002; Horritt et al., 2007):

$$F = \frac{A}{A + B + C} \tag{3.2}$$

where A is the number of cells correctly predicted by the model, B is the number of cells predicted as wet that is observed dry (overprediction), and C is the number of cells predicted as dry that is observed wet (underprediction). F ranges from 0 to 1, the higher the better. As assumed in previous studies (e.g., Aronica et al., 2002; Pappenberger et al., 2007), only the cells with a simulated inundation depth greater than 20 cm are considered as flooded.

The evaluation of the simulated downstream water levels is conducted by using the observed time series of flood water levels at the downstream end of the river reach. The calibration focuses on the peak hours of the water stage hydrograph, starting on December 7, 2006 at 4:00 a.m. and ending 127 h later, which is also the time of the satellite overpass. The root mean square error

(RMSE) is used to evaluate model errors for both LiDAR and SRTM-based model.

3.4 The effect of topography resolution on inundation modeling

To better distinguish between the impact of the resolution and the accuracy of topographical input data, we first conduct a numerical experiment to isolate the resolution effect: the LiDAR DEM is aggregated into 80-m resolution DEM, which is similar to the SRTM resolution (i.e., 75 m). Then the subgrid LiDAR-based model (80 m of resolution) in which the channel has the same width, friction, and bed elevation to the LiDAR-based model (20 m of resolution) is built. The SRTM-based model (75 m of resolution) is used for comparison. The other model parameters among three models are identical.

The flood extents simulated by three models are compared to the flood extent derived from the ERS2-SAR image. The value of performance measure, F, is shown in Table 3.1. The coarse resolution LiDAR-based model performs slightly worse than the high resolution one (with 0.01 difference in terms of F), whereas the performance is much higher than the SRTM-based model (with 0.271 difference in terms of F). This shows that coarse resolution LiDAR-based model can simulate the flood extent equally well as the high resolution LiDAR-based model. The coarse resolution does not degrade the model performance, whereas the vertical accuracy of floodplain cells might play an important role. Thus, we focus on the effect of DEM vertical accuracy on flood extent and downstream water level predictions in the following experiments.

3.5 Uncertainty analysis within a generalized likelihood uncertainty estimation framework

To investigate the usefulness of SRTM data to support hydraulic modeling, the effects of topography uncertainty are evaluated within the generalized likelihood uncertainty estimation (GLUE, Beven and Binley, 1992) framework. GLUE is a simple and pragmatic methodology, which uses Monte Carlo simulations to produce parameter distributions and uncertainty bounds conditioned on available data. GLUE has been widely used in environmental

TABLE 3.1 Comparison of three floodplain models.

	LiDAR-based model (80 m)	LiDAR-based model (20 m)	SRTM-based model (75 m)
F	0.781	0.791	0.510

SRTM, shuttle radar topography mission.

modeling (e.g., Aronica et al., 1998; Romanowicz and Beven, 1998; Beven and Freer, 2001). It is worth noting that a number of authors (Montanari, 2005; Mantovan and Todini, 2006; Stedinger et al., 2008) showed that the GLUE methodology does not formally follow the Bayesian approach in estimating the posterior probabilities of parameters and of the output distribution. Also, a number of subjective decisions have to be made in GLUE, for example, the priori distribution and feasible range of each parameter (generalized) likelihood function for model evaluation, the threshold between behavioral and nonbehavioral simulations. It is therefore necessary to clarify each decision to be transparent and unambiguous.

The assumed ranges of parameters can have an influence on resulting uncertainties (Aronica et al., 1998). Thus, large parameter ranges, which cover the extreme feasible values, were used to overcome the potential issue of subjective choice (e.g., Aronica et al., 1998). Therefore, we keep the roughness parameter range sufficiently large. Both Manning's channel and flood-plain roughness coefficients are sampled randomly from the uniform distribution between 0.015 and 0.150 $\mathrm{m}^{1/3}\mathrm{s}^{-1}$ due to the lack of information regarding the priori distribution as well as the feasible range of parameters. A similar parameter range was also used by Stephens et al. (2014) for the same study area. The range of average bed slopes is calculated from the two topographic data sets: the upper bound of the bed slope is calculated based on the reach from Fardon to Iron Bridge, whereas the lower bound is calculated based on the reach from the confluence to Iron Bridge for both LiDAR and SRTM-based model (Table 3.2).

The objective function (i.e., *F* and RMSE) values for each parameter set (i.e., Manning's coefficients in channel (n_{ch}), Manning's coefficients on floodplain *(nfp),* and water surface slope *(Sl)*) are calculated to derive the generalized likelihoods, which are positive values with the summation of 1 (Wagener et al., 2001). The likelihood measure can be used to weight each model realization. The behavioral models can be selected by rejecting the simulations that underperform a user-defined threshold or a percentage of simulations. In this study, the best 10% of the realizations are assumed as behavioral models and then used to produce probabilistic inundation maps.

TABLE 3.2 Bed slope calculated from two topographic data.

	Farndon to Iron Bridge	Confluence to Iron Bridge
LiDAR-based model	0.0002	0.00002
SRTM-based model	0.0012	0.0002

SRTM, shuttle radar topography mission.

Given the simulation results for the *jth* computational cell of $w_{ij} = 1$ for wet and $w_{ij} = 0$ for dry, the probabilistic inundation map is produced using Eq. (3.3):

$$M_j = \frac{\sum_i L_i w_{ij}}{\sum_i L_i} \tag{3.3}$$

where Mj indicates a weighted average flood state for the *jth* cell and L_i is the likelihood weight assigned for each simulation *i*. The posterior parameter distributions (PPDs) of both two models are plotted as well.

3.6 Results and discussion

We conducted 1000 simulations for LiDAR and SRTM-based models within the GLUE framework (see above). Two performance measures are evaluated according to two types of observations. The dotty plots are generated to show the parameter uncertainty given alternative performance measures and data sets for both LiDAR and SRTM-based model.

Fig. 3.2A and B shows that the performance measure of LiDAR-based model increases as the n_{ch} and n_{fp} increase when conditioned on flood extent data for the small n_{ch} and n_{fp} values (below 0.05). The performance
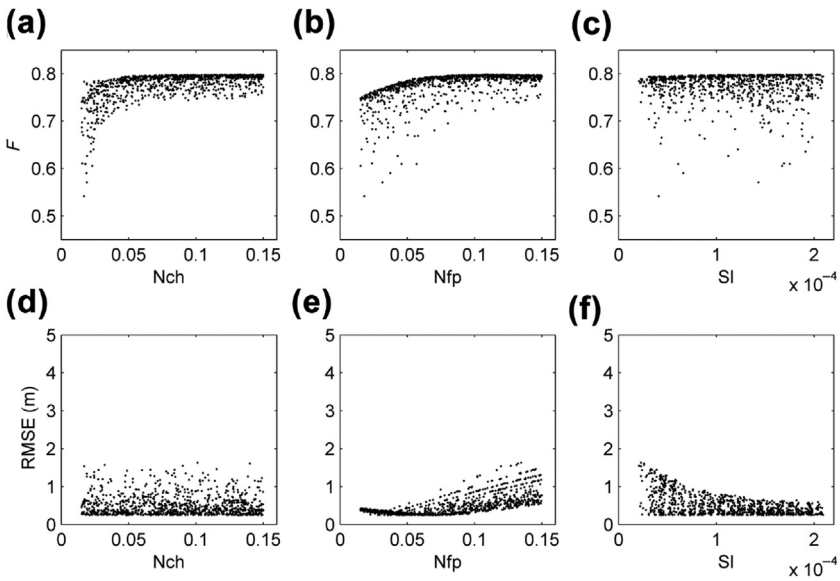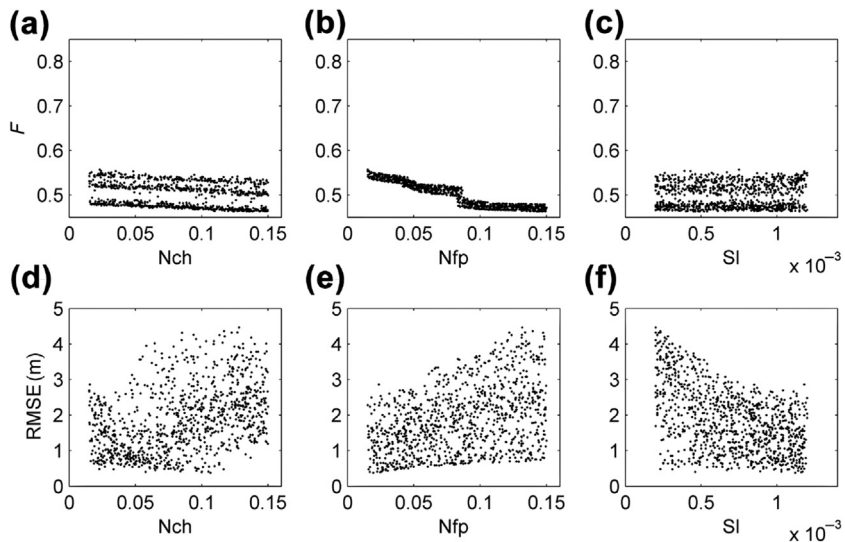

FIGURE 3.2 (A)−(C) Performance measure F for LiDAR-based model conditioned on ERS2-SAR flood image. (D)−(F) Performance measure root mean square error (RMSE) for LiDAR-based model conditioned on downstream water stage.

measure begins to remain unchanged for the larger n_{ch} and n_{fp} values. It is found out that there is a tendency to generally underestimate the flood extent for smaller Manning's coefficients. The simulated inundation extent is, as expected, increasing when n_{ch} and n_{fp} are increasing.

It is difficult to observe the optimal *SI* when conditioned on flood-extent data as good simulations occur across the whole range of parameter values (Fig. 3.2C). The flood extent is affected by the back-water effect and therefore related to the downstream water slope *SI*. However, the influence of backwater to flood extent in this case is limited as the floodplain acts as a "valley-filling" case, whereby, once the valley is filled by flood water, increases of water depth do not lead to significant differences in flood extent (Hunter et al., 2005).

The sensitivity to parameters nf_p and *SI* is assessed also by conditioning the model on downstream water levels (Fig. 3.2E and F). The RMSE is increasing when *nfp* is increasing with the optimal value around 0.05. The RMSE is decreasing when *SI* is increasing (Fig. 3.2F). The effects of the two parameters are compensated with each other (e.g., when *SI* is increasing, one can keep almost the same water level but increase nf_p). The sensitivity of *SI* is clearly visible as conditioned on water stage information, as expected. The predicted downstream water levels are strongly affected by the assumed water-surface slope.

In Fig. 3.3C, the average performance measure remains stationary with the change of *SI* when the SRTM-based model is conditioned on flood-extent data.

FIGURE 3.3 (A)–(C) Performance measure *F* for shuttle radar topography mission (SRTM)-based model conditioned on ERS2-SAR flood image. (D)–(F) Performance measure root mean square error (RMSE) for SRTM-based model conditioned on downstream water stage.

A clearly decreasing performance as *njp* is increasing (Fig. 3.3B). A similar trend also occurs for n_{ch} (Fig. 3.3A). The SRTM-based model essentially overestimates the flood extent (with very few underprediction cells), even with the optimal parameter sets. This is shown by the fact that the performance measure (F) keeps dropping while n_{ch} and nf_p are increasing due to the fact that the simulated inundation extent keeps increasing, which results in more overprediction.

The sensitivity of SRTM-based model conditioned on downstream water stage (Fig. 3.3D−F) is overall larger than LiDAR-based model. The realizations with high performance (low RMSE) are more concentrated in an area with the small values of n_{ch} and n_{fp} rather than the high ones. Similarly to the LiDAR-based model, the SRTM-based model performs better with larger *SI* values (Figs. 3.2F and 3.3F).

Fig. 3.4B and E shows that, when conditioned on downstream water stages, the best realizations are obtained with small Manning's floodplain roughness values (around 0.05), whereas high-performance realizations are found for higher Manning's floodplain values, when the model is conditioned on flood extent. The PPD for water surface slope, when conditioned on flood extent, and Manning's channel coefficients, when conditioned on water stage, are found nearly uniformly distributed for the LiDAR-based model (Fig. 3.4C and D). If all the realizations are taken as behavioral, we might conclude that the
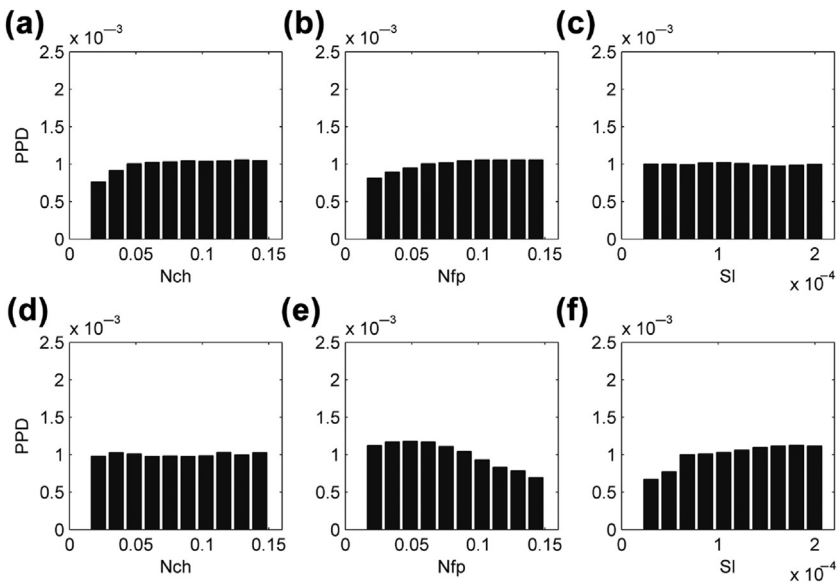

FIGURE 3.4 (A)−(C) Posterior parameter distribution (PPD) for LiDAR-based model conditioned on ERS2-SAR flood image. (D)−(F) PPD for LiDAR-based model conditioned on downstream water stage.

simulations conditioned on hydrometric data (i.e., water-stage time series) may not predict the flood extent properly for LiDAR-based model (Fig. 3.4A−F). However, the performances are very different after the rejection of nonbehavioral simulations. Fig. 3.5 (upper panel) shows the flood extent predicted by the best 10% simulations, conditioned on downstream
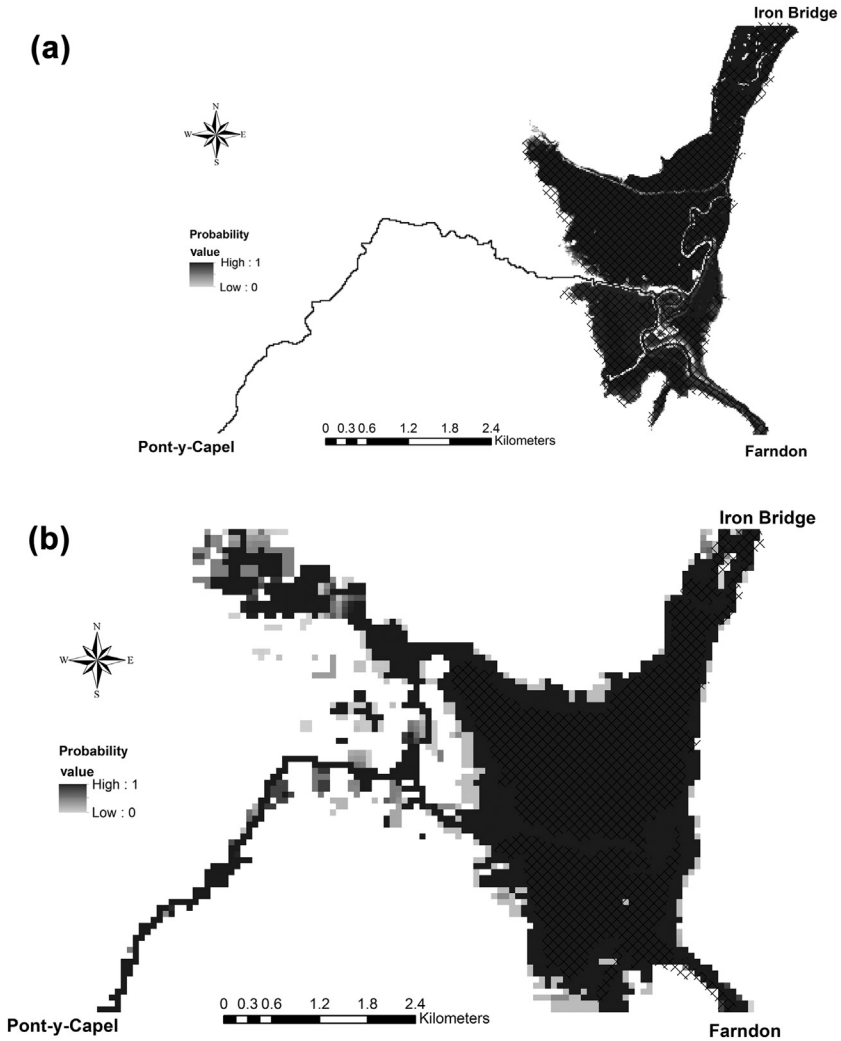
FIGURE 3.5 ERS2-SAR flood imagery (crosshatch) and probabilistic inundation map of 2006 event (from black, 1, to white, 0) with behavior simulations conditioned on downstream water stage: (A) LiDAR-based model; (B) shuttle radar topography mission-based model.
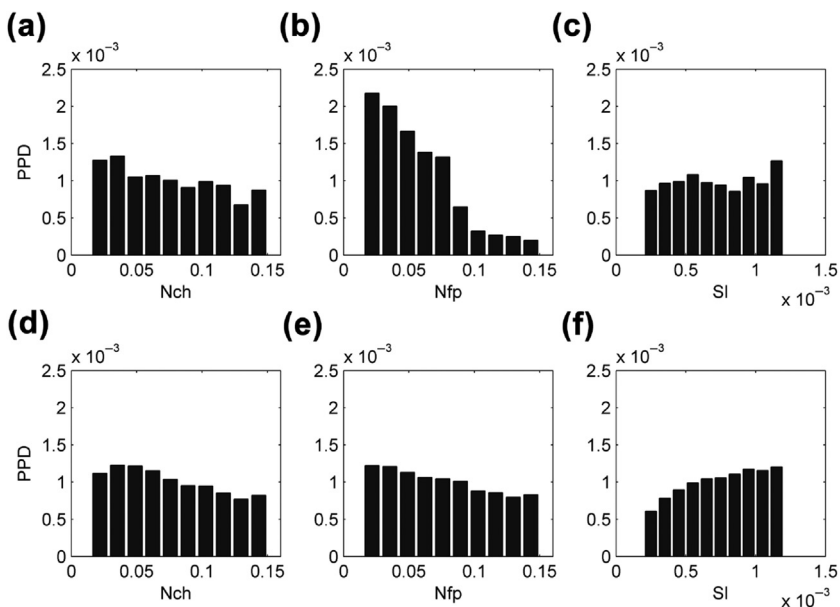
TABLE 3.3 Performance measure F of two models.

	Performance measure F	
Average of best 10% simulations conditioned on water stage	Average of best 10% simulations conditioned on ERS2-SAR	Best of 1000 Simulations
LiDAR-based 0.771 model	0.797	0.799
SRTM-based 0.524 model	0.543	0.557

SRTM, shuttle radar topography mission.

water stages of which the average performance measure (F) is 0.771, given the best F among all 1000 simulations is 0.799 (see Table 3.3).

In Fig. 3.6, the PPD shows the performance of parameters for SRTM-based model is rather similar between the two performance measures (i.e., F and RMSE). This indicates that it might get relatively satisfactory predictions of flood extent when the SRTM-based model is conditioned on water stage data. It also shows SRTM-based model might be more flexible in

FIGURE 3.6 (A)–(C) Posterior parameter distribution (PPD) for shuttle radar topography mission (SRTM)-based model conditioned on ERS2-SAR flood image. (D)–(F) PPD for SRTM-based model conditioned on downstream water stage.

conditioning on different data sets than LiDAR-based model. The model performances after the rejection of nonbehavioral simulations are also shown in Fig. 3.5 (lower panel). The probabilistic inundation map of the best 10% simulations conditioned on water stage, of which the average performance measure (F) is 0.524, compares with the best F of 0.557 among all 1000 simulations (Table 3.3).

Figs. 3.2 and 3.3 show that the LiDAR-based model performs better than the SRTM-based model in predicting flood extent as well as the downstream water stage. This shows how the performance of hydraulic models can be affected by topographic errors. The prediction of downstream water stages shows a mean RMSE of 1.853 m for SRTM-based model and 0.504 m for the LiDAR-based model. Considering the predicted water stage is obviously affected by the channel-bed elevation, the poor performance of the SRTM-based model is expected. On the other hand, the mean F of the best 10% realizations conditioned on ERS2-SAR is 0.543 for SRTM-based model and 0.797 for LiDAR-based model (Table 3.3). Despite this large difference, getting a performance above 50% in simulating flood extent is a reasonably good result for using SRTM topography to support the hydraulic modeling of a small−medium-sized river.

3.7 Conclusions

This chapter presents an evaluation of the potential usefulness of SRTM topography in supporting models predicting flood extent as well as downstream water stages, by taking into account parameter uncertainty within a GLUE framework. The topographic uncertainty is estimated by comparing the SRTM-based model to a model based on high-resolution topography (i.e., LiDAR plus channel survey). The ERS2-SAR flood imagery and downstream time series of water stages of the 2006 flood event are used to constrain model uncertainty. Roughness coefficients in channel and floodplain as well as the water surface slope are sampled uniformly within their parameter space. The effect of water surface slope in affecting flood extent and downstream water stages is quantified. The ability of a 2D flood inundation model conditioned on water stage to simulate flood extent is also evaluated.

The SRTM-based model performs poorly for the downstream water stage predictions, but it captures the majority of the inundation patterns. In addition, similar optimal parameters for the SRTM-based model conditioned on flood extent or water stage are encouraging. However, to generalize these findings, SRTM data should be tested on more case studies.

It is also shown that the optimal parameters are rather different when the LiDAR-based model is conditioned on either the flood extent or water stages. However, when behavioral simulations are conditioned on water stage, predictions of flood extent prediction are rather good. This is likely due to the fact that the differences in water levels do not imply changes in flood extent.

The water surface slope used as downstream boundary condition is found to have a negligible impact on flood extent predictions with the LiDAR-based model and a limited impact on flood-extent predictions with the SRTM-based model. In contrast, the downstream water surface slope is found to significantly affect water stage predictions of both models. This finding suggests that water-surface slope has to be selected with caution when one of the purposes of the hydraulic model is the prediction of downstream water stages and design flood profiles.

Acknowledgments

References

Aronica, G., Hankin, B., Beven, K., 1998. Uncertainty and equifinality in calibrating distributed roughness coefficients in a flood propagation model with limited data. Adv. Water Resour. 22 (4), 349−365.

Aronica, G., Bates, P.D., Horritt, M.S., 2002. Assessing the uncertainty in distributed model predictions using observed binary pattern information within GLUE. Hydrol. Process. 16 (10), 2001−2016.

Bates, P.D., 2004. Remote sensing and flood inundation modelling. Hydrol. Process. 18, 2593−2597.

Bates, P.D., 2012. Integrating remote sensing data with flood inundation models: how far have we got? Hydrol. Process. 26 (16), 2515−2521.

Bates, P.D., De Roo, A.P.J., 2000. A simple raster-based model for flood inundation simulation. J. Hydrol. 236 (1−2), 54−77.

Bates, P.D., Horritt, M.S., Aronica, G., Beven, K., 2004. Bayesian updating of flood inundation likelihoods conditioned on flood extent data. Hydrol. Process. 18 (17), 3347−3370.

Bates, P.D., Horritt, M.S., Fewtrell, T.J., 2010. A simple inertial formulation of the shallow water equations for efficient two-dimensional flood inundation modelling. J. Hydrol. 387 (1−2), 33−45.

Beven, K.J., Binley, A., 1992. The future of distributed models: model calibration and uncertainty prediction. Hydrol. Process. 6, 279−298.

Beven, K., Freer, J., 2001. Equifinality, data assimilation, and uncertainty estimation in mechanistic modelling of complex environmental systems using the GLUE methodology. J. Hydrol. 249 (1−4), 11−29.

Brandimarte, L., Di Baldassarre, G., 2012. Uncertainty in design flood profiles derived by hydraulic modelling. Hydrol. Res. 43 (6), 753−761.

de Moel, H., van Alphen, J., Aerts, J.C.J.H., 2009. Flood maps in Europe — methods, availability and use. Nat. Hazards Earth Syst. Sci. 9 (2), 289−301.

Di Baldassarre, G., Montanari, A., 2009. Uncertainty in river discharge observations: a quantitative analysis. Hydrol. Earth Syst. Sci. 13 (6).

Di Baldassarre, G., Uhlenbrook, S., 2012. Is the current flood of data enough? A treatise on research needs for the improvement of flood modelling. Hydrol. Process. 26 (1), 153−158.

Di Baldassarre, G., Schumann, G., Bates, P.D., Freer, J.E., Beven, K.J., 2010. Flood-plain mapping: a critical discussion of deterministic and probabilistic approaches. Hydrol. Sci. J. 55 (3), 364−376.

Di Baldassarre, G., Schumann, G., Brandimarte, L., Bates, P., 2011. Timely low resolution SAR imagery to support floodplain modelling: a case study review. Surv. Geophys. 32 (3), 255−269.

Falorni, G., Teles, V., Vivoni, E.R., Bras, R.L., Amaratunga, K.S., 2005. Analysis and characterization of the vertical accuracy of digital elevation models from the Shuttle Radar Topography Mission. J. Geophys. Res. Earth Surf. 110 (F2), F02005.

García-Pintado, J., Neal, J.C., Mason, D.C., Dance, S.L., Bates, P.D., 2013. Scheduling satellite-based SAR acquisition for sequential assimilation of water level observations into flood modelling. J. Hydrol. 495 (0), 252−266.

Horritt, M.S., Bates, P.D., 2002. Evaluation of 1D and 2D numerical models for predicting river flood inundation. J. Hydrol. 268 (1—4), 87−99.

Horritt, M.S., Di Baldassarre, G., Bates, P.D., Brath, A., 2007. Comparing the performance of a 2-D finite element and a 2-D finite volume model of floodplain inundation using airborne SAR imagery. Hydrol. Process. 21 (20), 2745−2759.

Hunter, N.M., Bates, P.D., Horritt, M.S., De Roo, A.P.J., Werner, M.G.F., 2005. Utility of different data types for calibrating flood inundation models within a GLUE framework. Hydrol. Earth Syst. Sci. 9 (4).

Hunter, N.M., Bates, P.D., Horritt, M.S., Wilson, M.D., 2007. Simple spatially-distributed models for predicting flood inundation: a review. Geomorphology 90 (3 —4), 208−225.

Jarvis, A., Reuter, H.I., Nelson, A., Guevara, E., 2008. Hole-Filled SRTM for the Globe Version 4. International Centre for Tropical Agriculture (CIAT). Available from: http://srtm.csi.cgiar.org.

LeFavour, G., Alsdorf, D., 2005. Water slope and discharge in the Amazon River estimated using the shuttle radar topography mission digital elevation model. Geophys. Res. Lett. 32 (17), L17404.

Mantovan, P., Todini, E., 2006. Hydrological forecasting uncertainty assessment: incoherence of the GLUE methodology. J. Hydrol. 330 (1—2), 368−381.

Matgen, P., Schumann, G., Henry, J.B., Hoffmann, L., Pfister, L., 2007. Integration of SAR-derived river inundation areas, high-precision topographic data and a river flow model toward near real-time flood management. Int. J. Appl. Earth Obs. Geoinf. 9 (3), 247−263.

Montanari, A., 2005. Large sample behaviors of the generalized likelihood uncertainty estimation (GLUE) in assessing the uncertainty of rainfall-runoff simulations. Water Resour. Res. 41 (8), W08406.

Neal, J., Schumann, G., Bates, P.D., 2012. A subgrid channel model for simulating river hydraulics and floodplain inundation over large and data sparse areas. Water Resour. Res. 48, W11506.

Neal, J., Keef, C., Bates, P., Beven, K., Leedal, D., 2013. Probabilistic flood risk mapping including spatial dependence. Hydrol. Process. 27 (9), 1349−1363.

Pappenberger, F., Matgen, P., Beven, K.J., Henry, J.-B., Pfister, L., Fraipont de, P., 2006. Influence of uncertain boundary conditions and model structure on flood inundation predictions. Adv. Water Resour. 29 (10), 1430−1449.

Pappenberger, F., Frodsham, K., Beven, K., Romanowicz, R., Matgen, P., 2007. Fuzzy set approach to calibrating distributed flood inundation models using remote sensing observations. Hydrol. Earth Syst. Sci. 11 (2).

Rabus, B., Eineder, M., Roth, A., Bamler, R., 2003. The shuttle radar topography mission—a new class of digital elevation models acquired by spaceborne radar. ISPRS J. Photogrammetry Remote Sens. 57 (4), 241−262.

Rodríguez, E., Morris, C.S., Belz, J.E., 2006. A global assessment of the SRTM performance. Photogramm. Eng. Rem. Sens. 72 (3), 249−260.

Romanowicz, R., Beven, K., 1998. Dynamic real-time prediction of flood inundation probabilities. Hydrol. Sci. J. 43 (2), 181−196.

Samuels, P., 1989. Backwater length in rivers. Proc. Inst. Civ. Eng. 87, 571−582.

Sanders, B.F., 2007. Evaluation of on-line DEMs for flood inundation modeling. Adv. Water Resour. 30 (8), 1831−1843.

Schumann, G., Matgen, P., Cutler, M.E.J., Black, A., Hoffmann, L., Pfister, L., 2008. Comparison of remotely sensed water stages from LiDAR, topographic contours and SRTM. ISPRS J. Photogrammetry Remote Sens. 63 (3), 283−296.

Schumann, G., Di Baldassarre, G., Bates, P.D., 2009. The utility of spaceborne radar to render flood inundation maps based on multialgorithm ensembles. Geosci. Remote Sens., IEEE Trans. 47 (8), 2801−2807.

Schumann, G., Di Baldassarre, G., Alsdorf, D., Bates, P.D., 2010. Near real time flood wave approximation on large rivers from space: application to the River Po. Italy. Water Resour. Res. 46.

Schumann, G., Neal, J.C., Phanthuwongpakdee, K., Voisin, N., Aspin, T., 2012. Assessing forecast skill of a large scale 2D inundation model of the Lower Zambezi River with multiple satellite data sets. In: XIX International Conference on Water Resources. University of Illinois at Urbana-Champaign.

Stedinger, J.R., Vogel, R.M., Lee, S.U., Batchelder, R., 2008. Appraisal of the generalized likelihood uncertainty estimation (GLUE) method. Water Resour. Res. 44, W00B06.

Stephens, E., Schumann, G., Bates, P.D., 2014. Problems with binary pattern measures for flood model evaluation. Hydrol. Process. 28 (18), 4928−4937.

Van Alphen, J., Martini, F., Loat, R., Slomp, R., Passchier, R., 2009. Flood risk mapping in Europe, experiences and best practices. J. Flood Risk Manage. 2 (4), 285−292.

Wagener, T., Lees, M.J., Wheater, H.S., 2001. A toolkit for the development and application of parsimonious hydrological models. Math. Models Large Watershed Hydrol. 1, 87−136.

Wang, Y., Liao, M., Sun, G., Gong, J., 2005. Analysis of the water volume, length, total area and inundated area of the Three Gorges Reservoir, China using the SRTM DEM data. Int. J. Rem. Sens. 26 (18), 4001−4012.

Yan, K., Di Baldassarre, G., Solomatine, D.P., 2013. Exploring the potential of SRTM topographic data for flood inundation modelling under uncertainty. J. Hydroinf. 15 (3), 849−861.